ACS APPLIED MATERIALS & INTERFACES

www.acsami.org

Research Article

Liquid-Phase Exfoliation of Bismuth Telluride Iodide (BiTeI): Structural and Optical Properties of Single-/Few-Layer Flakes

Gabriele Bianca, Chiara Trovatello, Attilio Zilli, Marilena Isabella Zappia, Sebastiano Bellani,* Nicola Curreli, Irene Conticello, Joka Buha, Marco Piccinni, Michele Ghini, Michele Celebrano, Marco Finazzi, Ilka Kriegel, Nikolas Antonatos, Zdeněk Sofer, and Francesco Bonaccorso*

Cite This: *ACS Appl. Mater. Interfaces* 2022, 14, 34963−34974

Read Online

ACCESS | Metrics & More | Article Recommendations | Supporting Information

ABSTRACT: Bismuth telluride halides (BiTeX) are Rashba-type crystals with several potential applications ranging from spintronics and nonlinear optics to energy. Their layered structures and low cleavage energies allow their production in a two-dimensional form, opening the path to miniaturized device concepts. The possibility to exfoliate bulk BiTeX crystals in the liquid represents a useful tool to formulate a large variety of functional inks for large-scale and cost-effective device manufacturing. Nevertheless, the exfoliation of BiTeI by means of mechanical and electrochemical exfoliation proved to be challenging. In this work, we report the first ultrasonication-assisted liquid-phase exfoliation (LPE) of BiTeI crystals. By screening solvents with different surface tension and Hildebrandt parameters, we maximize the exfoliation efficiency by minimizing the Gibbs free energy of the mixture solvent/BiTeI crystal. The most effective solvents for the BiTeI exfoliation have a surface tension close to 28 mN m^{-1} and a Hildebrandt parameter between 19 and 25 $MPa^{0.5}$. The morphological, structural, and chemical properties of the LPE-produced single-/few-layer BiTeI flakes (average thickness of ∼3 nm) are evaluated through microscopic and optical characterizations, confirming their crystallinity. Second-harmonic generation measurements confirm the non-centrosymmetric structure of both bulk and exfoliated materials, revealing a large nonlinear optical response of BiTeI flakes due to the presence of strong quantum confinement effects and the absence of typical phase-matching requirements encountered in bulk nonlinear crystals. We estimated a second-order nonlinearity at 0.8 eV of $|\chi^{(2)}| \sim 1$ nm V^{-1}, which is 10 times larger than in bulk BiTeI crystals and is of the same order of magnitude as in other semiconducting monolayers (e.g., MoS_2).

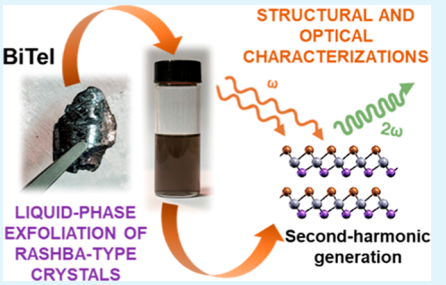

KEYWORDS: *two-dimensional materials, liquid-phase exfoliation, Rashba effect, nonlinear optics, second-harmonic generation*

INTRODUCTION

Layered ternary bismuth telluride halides (BiTeX, X = Cl, Br, or I) have recently gained research interest because of their polar non-centrosymmetric or non-symmorphic structures coupled with sizeable spin−orbit interaction (SOI) effects,[1−5] resulting from the mixed ionic−covalent character of the compound[6] and the presence of heavy Bi atoms.[2] Such distinctive features lift the Kramer's spin degeneracy of both the three-dimensional (3D) bulk[1,2,7−9] and two-dimensional (2D) surface states.[3,10−19] This leads to the momentum-dependent spin splitting in the band structure in the absence of an external magnetic field, originating from both bulk and structural inversion asymmetries (i.e., Dresselhaus and Rashba effects), as described by a 2D electron gas Rashba−Bychkov model[20] or its phenomenological extensions.[21,22] Ab initio calculations of the band structure and angle-resolved photoemission spectroscopy studies on BiTeX have shown that direct consequences of the Rashba effect are complex Fermi surfaces[23−25] and other related physical phenomena. The most intriguing ones are multiple-frequency Shubnikov−de Haas oscillations,[24,26−29] temperature-robust Dirac Landau level structures,[30] spin-polarized magneto photocurrents,[31] and pressure-induced topological quantum phase transitions toward non-trivial topological insulators with material side-dependent Dirac states.[28,29,32−37] The evolution toward new quantum phases can lead to the fascinating pressure-dependent bulk photovoltaic effect[38] and pressure-induced superconductivity.[33,34] The surface state splitting off from the bulk bands in the presence of a potential change within the near-surface layer[3,10−14] and the rational control of the spin information in BiTeX through the chemical potential-/doping-/mechanical stress-modulated Rashba effect represent new paradigm shifts in the realization of spin(orbi)tronic (spin devices,[1,10,39−44] including spin field-/Hall-effect transistors,[22] spin−orbit

Received: May 1, 2022
Accepted: July 4, 2022
Published: July 25, 2022

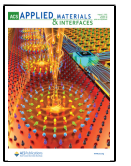

torque devices,[45] spin injectors,[46] and "Rashba p−n junctions")[10,47] as well as thermoelectric[48−51] and piezoelectric systems[52] with tunable nonlinear optical properties[53] and even electrocatalytic materials.[54]

In this context, pioneering[1,10,23,] and recent[22,55,56] theoretical studies coupled with experimental observations[1] revealed that BiTeI exhibits a giant Rashba spin splitting of hundreds of meV (i.e., ∼400 meV),[1] which is among the largest reported so far. Its layered structure is built of ionically bound $(BiTe)^+$ and I^- layers,[6,52] forming BiTeI trilayers that are held together by van der Waals forces.[6,52] Consequently, the plane between Te and I is a natural cleavage plane of the crystal, revealing Te- or I-terminated surfaces.[10,16,17] Along with the rapid advances in designing artificial van der Waals heterostructures by stacking 2D materials,[56−58,] exfoliated BiTeI flakes might be architectural components in functional quantum systems,[59−61] including the realization of time-reversal invariant topological insulating phases,[62,63] such as the predicted $Bi_2Te_2I_2$ sextuple layer composed by Te-faced BiTeI.[64] The realization of 2D materials with giant Rashba effects is a fascinating strategy to enable nanometer-scale spintronics operating at room temperature,[65−67] as well as nanoscale piezoelectric[68] and nonlinear optical applications.[69] More generally, thanks to their morphology and the plethora of their distinctive properties, 2D materials are foreseen as the ultimate building blocks to produce high-energy density (opto-) electronic devices with radically new functionality, aiming at expressing the "More than Moore" vision.[70−72]

Despite the layered structure of the bulk BiTeI and the predicted low cleavage energy to obtain its monolayer (*ca.* 90 meV/atom), which is comparable to the one reported for transition metal chalcogenides[73−75] and only *ca.* 60 meV/atom larger than the one of graphite,[76] the exfoliation of BiTeI in the single-/few-layer form remains challenging.[77] For example, BiTeI monolayers have been obtained through stripped gold exfoliation.[78] However, this methodology leads to a strong hybridization of the BiTeI monolayer with the Au substrate,[78] causing substantial modifications of the surface charge distribution onto the BiTeI surface.[78] Recently, multi-layer BiTeI flakes with thickness down to 10 nm and marginal topological etching of the iodine atoms have been produced through electrochemical exfoliation in *N*,*N*-dimethylformamide (DMF) with the aid of tetrabutylammonium or lithium cations.[54] For further advancement of the production and processing of the material class of 2D BiTeX, we report here for the first time the ultrasonication-aided liquid-phase exfoliation (LPE) of contamination-free BiTeI crystals. Notably, the exfoliation of Rashba-type layered polar crystals in liquid media expands the portfolio of solution-processed 2D materials, providing a novel type of functional ink for large-scale, high-speed, and cost-effective device manufacturing.[79−84]

In this work, the LPE of BiTeI crystals and the material dispersion stabilization are studied in 12 different solvents, allowing the Hildebrand and Hansen parameters of the BiTeI to be estimated. In fact, the material exfoliation yield is maximized by minimizing the Gibbs free energy of the solvent/crystal mixture.[85−87] Experimentally, this condition corresponds to matching the solubility parameters of the solvent with those of the crystal.[85−87] Moreover, it is important to identify a portfolio of different solvents for the exfoliation and processing of layered crystals.[79−81] In particular, the properties of the solvents (e.g., viscosity, vapor pressure, and boiling points, just to name a few) can impact the characteristics of the films obtained by casting/printing the exfoliated crystal dispersion to such an extent as to impede/allow eligible deposition techniques.[87,88] Our results indicate that the solvents with a surface tension (γ^{sol}) close to 28 mN m^{-1} (surface energy of 68 mJ m^{-2}) and a Hildebrandt parameter (δ_{Hild}) between 19 and 25 $MPa^{0.5}$ minimize the Gibbs free energy of the mixture solvent/BiTeI crystal.[85,89] In addition, the use of low-boiling point and high-vapor pressure solvents effectively avoids solvent residuals while eliminating the substrate interaction occurring during stripped gold exfoliation.[78] The morphological, structural, optical, and chemical properties of the exfoliated BiTeI flakes are evaluated here through a combination of microscopic and spectroscopic techniques, including nonlinear optical microscopy for second-harmonic generation (SHG). In fact, the concurrent spin−orbit coupling and structural inversion asymmetry of Rashba-type materials manifest themselves in nonlinear optical signals whose characteristics can be defined or even correlated to the Rashba strength of the material.[90,91] Consequently, 2D Rashba-type materials potentially provide novel nanometer-thin platforms for nonlinear optical studies and applications.[91−93] In addition, as shown for other polar 2D materials, such as group-IV metal monochalcogenides,[94] the lack of inversion symmetry and strong quantum confinement can lead to extraordinary second-order nonlinear optical effects.[94] Even more, since the nanometric thickness of exfoliated materials is much smaller than the second-harmonic (SH) coherence length, 2D materials bypass phase-matching constraints encountered in 3D nonlinear crystals.[95,96] Thus, we measure SHG from few-layer BiTeI flakes, which exhibit a large nonlinear optical response 10-fold more intense than that of bulk BiTeI crystals and of the same order of magnitude as that of group VI monolayer transition metal dichalcogenides (TMDs) ($|\chi^{(2)}|$ ∼0.1−1 nm V^{-1}).[95,97] These results prove the potential of LPE-produced BiTeI as a solution-processable low-dimensional Rashba-type material.

METHODS

Crystal Synthesis and Exfoliation. The crystals of BiTeI are synthesized by direct reaction of the atomic elements (Bridgman method), according to previous protocols.[54] Experimentally, stoichiometric amounts of bismuth, tellurium, and iodine (total weight of 6 g) are placed in a quartz glass ampule and sealed under high vacuum with an oxygen−hydrogen torch. Liquid nitrogen cooling is used during sealing to avoid iodine loss. The ampule is heated at 650 °C with a 1 °C min^{-1} heating rate, and after 6 h, it is cooled down to 400 °C with a 0.2 °C min^{-1} cooling rate. Finally, it is treated for 7 days at 400 °C and cooled down to room temperature overnight.

LPE of BiTeI Crystals. The BiTeI flakes are produced by LPE of bulk crystals,[75,98−102] followed by sedimentation-based separation[74,103−106] to remove unexfoliated material. In more detail, 50 mg of powdered bulk crystals are added to 50 mL of anhydrous solvents and ultrasonicated in a bath sonicator (Branson 5800 cleaner, Branson Ultrasonics) for 15 h. Various solvents are investigated, including water, isopropanol (IPA), acetonitrile, ethanol, methanol, *N*-methyl-2-pyrrolidone, *n*-hexane, DMF, chloroform, chlorobenzene, ethylene glycol, and acetone. The as-produced dispersions are ultracentrifuged at 700*g* (Optima XE 90 with a SW32Ti rotor, Beckman Coulter) for 20 min at 15 °C. Then, 80% of the supernatant is collected by pipetting, thereby obtaining the dispersions of the exfoliated materials.

Material Characterization. Scanning electron microscopy (SEM) imaging of the BiTeI crystals is carried out using a Optima XE 90 with a SW32Ti rotor), and elemental composition and mapping of the materials are obtained using an energy-dispersive X-

https://doi.org/10.1021/acsami.2c07704
ACS Appl. Mater. Interfaces 2022, 14, 34963−34974

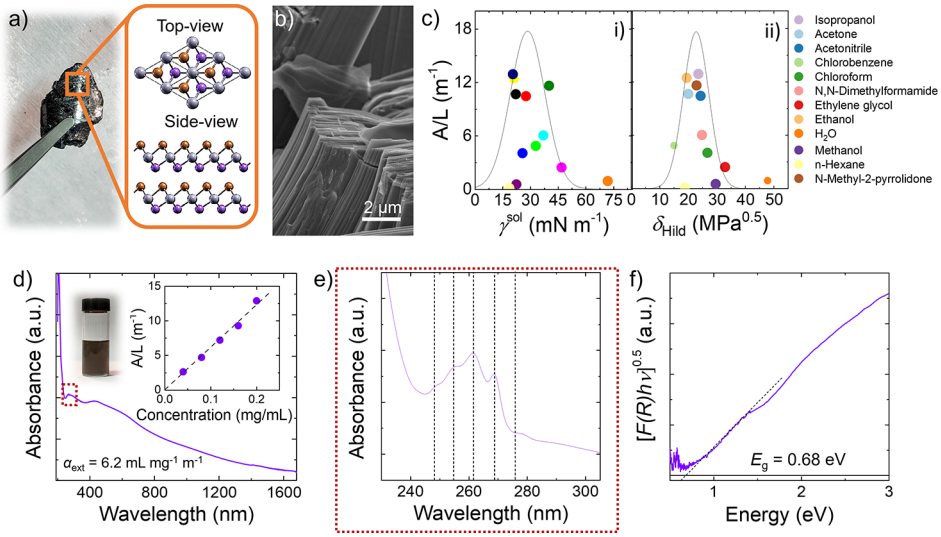

Figure 1. (a) Photograph of a BiTeI crystal produced through direct synthesis of its elements. The crystal structure (space group $P3m1$, no. 156) of the BiTeI crystals is also shown. (b) SEM image of a fragment of the BiTeI crystal, evidencing its layered structure. (c) Concentration (plotted as A/L) of the BiTeI flake dispersion produced through LPE dispersed in different solvents, plotted versus solvent γ^{sol} (panel i) and δ_{Hild} (panel ii). The continuous lines are Gaussian fits to data. (d) Absorbance spectra of the BiTeI flake dispersion in IPA. The photograph of the dispersion is also shown. The inset shows the Lambert–Beer plot of the BiTeI dispersion. (e) Absorbance spectra of the BiTeI flake dispersion in IPA in the ultraviolet, evidencing the fine structure of the optical transitions at high energy. (f) Tauc plot of a film of BiTeI flakes produced by spray coating the BiTeI flake dispersion in IPA onto a quartz substrate.

ray spectroscopy analyzer (X-Max^N) with a 20 mm^2 Si drift detector (X-Max^N SDD, Oxford Instruments) and the AZtecEnergy software. The measurements are performed using an electron beam in the range 5–10 kV. The samples are prepared by placing powdered crystals directly on a carbon conductive tape.

Bright-field transmission electron microscopy images of BiTeI flakes are acquired with a JEM 1011 (JEOL) transmission electron microscope TEM), equipped with a thermionic W filament operating at 100 kV. The samples are produced by depositing the BiTeI flake dispersion in IPA onto ultrathin C-on-holey C-coated Cu grids. The samples are rinsed with deionized water and subsequently dried overnight under vacuum before measurements. High-resolution TEM (HRTEM) characterization is performed using a JEOL JEM2200 image-corrected microscope operated at 200 kV and equipped with an in-column Omega energy filter and a Bruker Quantax 400 EDX system with a 60 mm^2 XFlash detector. The samples for these observations are prepared by drop-casting the dispersion of BiTeI flakes in IPA onto ultrathin C-coated Cu grids.

The atomic force microscopy (AFM) images are acquired with a NX10 AFM (Park System, Korea) by means of a non-contact cantilever PPP-NCHR 10 M (Nanosensors, Switzerland) having a tip diameter inferior to 10 nm, a resonance frequency of ~330 kHz, and a force constant of 42 N m^{-1}. The images are collected in the non-contact mode on an area of 5 × 5 μm^2 (1024 × 1024 data points), keeping the working setpoint above 70% of the free oscillation amplitude. The scan rate for the acquisition of the images is 0.2 Hz. The samples are prepared by drop-casting a 1:10 diluted dispersion of BiTeI flakes in IPA onto mica sheets (G250-1, Agar Scientific Ltd.) and heating to 100 °C for 15 min to dry the sample and remove adsorbates.

Absorbance spectroscopy measurements are performed on the dispersions of exfoliated BiTeI flakes with a Cary Varian 5000 spectrophotometer using quartz glass cuvettes. The as-produced dispersions of the exfoliated materials are diluted with the corresponding solvents at different ratios to determine the extinction coefficient of the BiTeI flakes. The extinction coefficient is determined by using the Beer–Lambert law, that is, $A = \alpha_{ext}cL$, where A is the absorbance at 700 nm, α_{ext} is the extinction coefficient, c is the concentration of the exfoliated materials, and L is the optical path length (1 cm).

Diffusive reflectance spectroscopy (DRS) measurements are performed using a Cary Varian 5000 spectrophotometer with an integrating sphere on films of BiTeI flakes deposited by spray coating onto quartz substrates. The diffusive reflectance (R) data are analyzed according to the Kubelka–Munk theory.[107] Experimentally, the optical band gap (E_g) is estimated by fitting the linear part of $[F(R)h\nu]^b$ versus $h\nu$ (Tauc Plot) with $[F(R)h\nu]^b = K(h\nu - E_g)$ (Tauc relation), where $F(R)$ is the Kubelka–Munk function, defined as $F(R) = (1 - R)^2/2R$, where h is Planck's constant, ν is the photon's frequency, and K is a proportionality constant.[107] The value of b indicates the type of electronic transitions differentiating between direct ($b = 2$) and indirect interband transitions ($b = 0.5$).[108] According to the electronic structure of the BiTeI bulk[1,10] and monolayer,[60,61,68] $b = 0.5$ is considered for the analysis of our sample.

X-ray diffraction (XRD) measurements are acquired with a PANalytical Empyrean using Cu Kα radiation. The samples for XRD are prepared by depositing powder of the BiTeI bulk crystal or BiTeI flakes (from IPA dispersion) onto Si/SiO$_2$ substrates.

Raman spectroscopy measurements are performed using a Renishaw microRaman inVia 1000 mounting an objective with 0.9 numerical aperture (NA), using an excitation wavelength of 514 nm and an incident power of 1 mW. For each sample, 50 spectra are collected to assess the reproducibility of the data. The samples are prepared by drop-casting the as-prepared BiTeI flakes dispersion onto Si/SiO$_2$ substrates and subsequently dried under vacuum.

Nonlinear optical measurements are performed on exfoliated BiTeI flakes drop-casted onto a SiO$_2$/Si substrate. The optical excitation is provided with a soliton mode-locked Er:Yb:glass laser (Onefive, Origami 15–80) emitting pulses of 160 fs duration and a 1551 nm center wavelength with a repetition rate of 80 MHz. The pump beam is focused onto the sample through a 0.85 NA dry objective (Nikon, CFI Plan Fluor 60XC) to a diffraction-limited illumination spot of about 1.8 μm diameter. The nonlinear emission is collected through the same objective in a back-scattering configuration, spectrally filtered at the SH wavelength (Figure S4), and detected using a single-photon avalanche diode (Micro Photon Devices, PD-050-CTD).

Statistical Analysis. Gwyddion 2.60 software was used to process the height profiles of the flakes imaged by AFM, while ImageJ software (NIH) was used to analyze the lateral size of the flakes imaged by BF-TEM. The lateral size of a flake was estimated as the mean of maximum and minimum lateral sizes of the flakes. OriginPro

https://doi.org/10.1021/acsami.2c07704
ACS Appl. Mater. Interfaces 2022, 14, 34963–34974

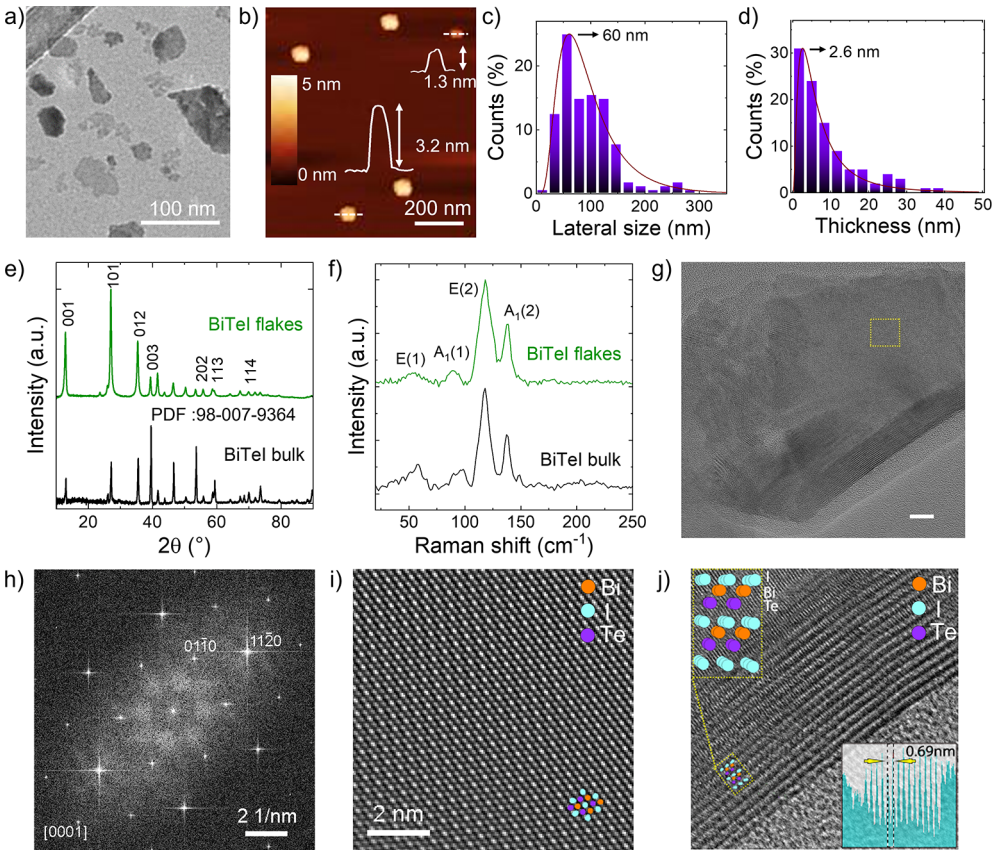

Figure 2. (a) BF-TEM and (b) AFM images of the BiTeI flakes produced through LPE of the BiTei crystal in IPA. (c) TEM statistical analysis of the lateral size of the BiTeI flakes (300 flakes). (d) AFM statistical analysis of the thickness of the BiTeI flakes (300 flakes). (e) XRD diffractograms and (f) Raman spectra (excitation wavelength of 514 nm) of BiTeI bulk crystals and flakes. The panels, respectively, report the diffraction peaks and the Raman modes attributed to the hexagonal *P*3*m*1 structure of the BiTeI crystals. (g) HRTEM image of a typical BiTeI flake with one edge folded onto itself (bottom bottom corner) and (h) the corresponding FFT confirming the single-crystalline nature of the flake and an exact [0001] orientation. (i) Close-up view of the area outlined by a rectangle in panel (g), showing the atomic arrangement as viewed from the [0001] direction. The atomic arrangement matches the expected atomic arrangement of BiTeI in the same orientation (a model is overlaid on top). (j) A folded edge of the flake reveals that it is 14 or 15 BiTeI unit cells thick. Individual monolayers spaced by 0.69 nm are clearly resolved.

9.1 software was also used to carry out the statistical analysis of the thickness and lateral size data. 300 BiTeI flakes on multiple AFM and TEM images were considered for the statistical analysis of the thickness and lateral size, respectively, of the BiTeI flakes.

RESULTS AND DISCUSSION

Hexagonal (space group *P*3*m*1, no. 156) BiTeI crystals are produced through direct synthesis of their elements, following protocols described in the literature (see the Methods section).[54] Figure 1a shows a photograph of a representative BiTeI crystal, together with its layered polar crystal structure built of ionically bound $(BiTe)^+$ and I^- layers (i.e., trilayers with I−Bi−Te stacking) tied together by van der Waals forces.[6,78] Figure 1b shows the SEM image of fragments of BiTeI crystals, whose layered structure is visible at their edges. The as-produced BiTeI crystals are further characterized by SEM-coupled energy-dispersive X-ray spectroscopy (EDS) (see Supporting Information, Figure S1), showing a nearly ideal BiTeI stoichiometry of 0.96:0.98:1. According to the predicted cleavage energy to obtain its monolayer (*ca.* 90 meV/atom) by cleaving the crystals along the Te−I planes, we initially investigate the LPE of the BiTeI bulk crystals by the prototypical ultrasonication method.[79,103,109] To further elucidate the exfoliation of BiTeX materials, we perform the ultrasonication-assisted LPE of the as-synthesized BiTeI crystals in 12 different solvents with diverse values of surface tension (γ^{sol}) and/or solubility parameters. Notably, the Gibbs free energy of the mixture solvent/layered material must be minimized to maximize the exfoliation of layered crystals and stabilize the resulting dispersion of exfoliated materials.[85−87,89] This condition is accomplished when the surface free energy of the material is equal to the surface free energy of the solvent, which can be calculated from γ^{sol}, that is,[89] $\gamma^{sol} = E^{sol}_{surf} - TS^{sol}_{surf}$, where E^{sol}_{surf} is the solvent surface energy, T is the absolute temperature, and S^{sol}_{surf} is the solvent surface entropy ($\sim 10^{-3}$ J m^{-2} K^{-1}).[89] Experimentally, the matching of the Hildebrand or Hansen solubility parameters of the layered materials with the ones of the solvent promotes the exfoliation processes.[85,86,110] The Hildebrand parameter (δ_{Hild}) is defined as the square root of the cohesive energy density, that is, $\delta_{Hild} = [(\Delta H_v - RT)/V_m]^{0.5}$, where ΔH_v is the enthalpy of vaporization, R is the ideal gas constant, and V_m is the molar volume.[86] Based on empirical considerations, solvents with δ_{Hild} values within a "small" range (e.g., within ±2 $MPa^{0.5}$ in polymer science) centered at the δ of the material are considered good solvents.[111] However, the δ_{Hild}-matching condition does not account for hydrogen bonding and polar interactions,[86] which can drastically affect the material solubility/dispersibility in a solvent.[112] Contrary to the Hildebrand model, the Hansen model predicts the solubility/dispersibility of material by referring to three

https://doi.org/10.1021/acsami.2c07704
ACS Appl. Mater. Interfaces 2022, 14, 34963−34974

parameters, which are the dispersion, polar, and hydrogen bonding components (δ_D, δ_P, and δ_H, respectively) of δ_{Hild}, as expressed by $\delta_{Hild}^2 = \delta_D^2 + \delta_p^2 + \delta_H^2$.[86,111] The Hansen parameters can be visualized in a 3D plot with $2\delta_D$, δ_P, and δ_H axes, resulting in a point for each solvent or material. According to the Hansen solubility criterion, suitable solvents are those which fall within a "small" sphere (e.g., a sphere with radius $\leq$8 $MPa^{0.5}$ in polymer science) centered at a point corresponding to the material.[111] Therefore, by plotting the extinction coefficients of the LPE-produced BiTeI dispersion as a function of γ^{sol} or the solubility parameters of the corresponding solvents, it is possible to estimate the surface free energy of the layered crystals, as well as their solubility parameters, from the maximum of the data distribution.[85−87] Figure 1c shows the A/L versus γ^{sol} and A/L versus δ_{Hild} plots, respectively, where A is the absorbance and L is the cell length. Being $A/L = \alpha_{ext}c$ (α_{ext} is the extinction coefficient, and c is the concentration of the exfoliated material, see the Methods section), the BiTeI exfoliation is maximized for solvents with γ^{sol} close to 28 mN m^{-1} (surface energy of 60 mJ m^{-2}) and δ_{Hild} between 19 and 25 $MPa^{0.5}$. This means that the surface free energy and δ_{Hild} of the BiTeI crystals are estimated within the range of values for the solvent capable of efficiently exfoliating the material. The plots of A/L versus Hansen parameters are shown in Figure S2. These data provide δ_P, δ_H, and δ_D values for BiTeI in the range of 6−17, 6−19, and 15−18 $MPa^{0.5}$, respectively. The exfoliation in IPA yielded a maximum concentration of ∼0.2 mg mL^{-1}. This means that the exfoliation yield, defined as the ratio between the weight of dispersed exfoliated flakes (after the centrifugation process, see details in the Methods section) and that of the starting bulk crystals (1 mg mL^{-1} concentration), is ∼20%. Figure 1d shows the absorption spectrum and the photograph of the BiTeI flake dispersion in IPA, which is stable over hundreds of hours (more than 1 month). The A/L plot (inset to Figure 1d) scales linearly with the concentration, allowing the estimation of α_{ext} at *ca.* 6.2 mL mg^{-1} m^{-1}. The absorption spectrum shows a long tail toward the near-infrared (NIR) region, in agreement with previous literature on both bulk[8,113] and exfoliated BiTeI. Absorption bands are observed around 435 nm (2.85 eV) and 265 nm (4.68 eV). These optical features have been almost disregarded in previous literature, which typically focused on the low-energy region (<1 eV).[8] Notably, in an isolated Bi^{3+} ion, the $6s^2$ configuration exhibits the $^1S_0$ ground state, while the $6s^1$ $6p^1$ configuration generates four excited states: three $^3P_{0,1,2}$ states and one $^1P_1$ state.[114] The absorption band at 265 nm cannot be assigned either to the $^1S_0 \rightarrow {}^3P_{0,1,2}$ spin-forbidden transitions or to $^1S_0 \rightarrow {}^1P_1$ since 265 nm is not compatible with any wavelength at which those transitions are expected.[114−116] Moreover, Figure 1e shows that this high-energy band is the overlap of at least five different contributions equally spaced by 0.13 eV. We speculate that such a band originates from the excitation of one electron from Bi^{3+} 5d orbitals to Bi^{3+} 6p orbitals. This excitation should produce several excited states in the Bi^{3+} ion, all having the same $5d^96s^26p^1$ electronic configuration. The fine structure of BiTeI flakes may depend on the crystalline field and SOIs and may also be influenced by the Rashba magnetic field. The E_g value of the BiTeI flakes is estimated through DRS using the Kubelka−Munk theory of diffusive reflectance (R) (see additional details in the Methods section).[107] Figure 1f shows the corresponding Tauc plot, considering BiTeI flakes as indirect band gap materials (i.e., in the Tauc relation described in the Methods section, b = 0.5). From the Tauc relation, the E_g of BiTeI flakes is estimated as 0.68 eV. This value is similar to those computed by DFT simulations for monolayer BiTeI (electronic transition near the Γ point),[60,61,68,78] suggesting that our films are mainly made of single and few-layer flakes (see additional discussion hereafter). The low-energy ($<E_g$) signal is attributed to intraband transitions occurring between spin-conduction bands, which involve electronic states with opposite spin orientations.[8,113]

The morphology of the LPE-produced BiTeI flakes in IPA is evaluated through AFM and TEM measurements. Figure 2a shows a TEM image of representative flakes with irregular shapes. Figure 2b reports an AFM image of representative flakes, whose height profiles correspond to flake thicknesses between 1 and 4 nm. The statistical analysis of the lateral size and thickness of the BiTeI flakes (Figure 2c,d) shows that the data follow a log-normal distribution peaked at ∼60 and ∼2.6 nm, respectively. These data indicate that the exfoliated sample mainly consists of single-/few-layer BiTeI flakes. Notably, previous studies reported an experimental AFM thickness of the BiTeI monolayer on the Au substrate in the range of 8.5 ± 1.2 Å.[78] Since BiTeI monolayers strongly interact with Au (binding energy of 681 and 969 meV for I and Te-terminations of BiTeI, respectively),[78] this value is close to bulk lattice parameters of BiTeI in the out-of-plane direction, that is, 6.5 Å or 6.9 Å.[6] In our case, by considering the distance between BiTeI flakes and the mica substrate, the lowest measured thicknesses (∼1 nm) are attributed to BiTeI monolayers. The structural properties of the BiTeI flakes are evaluated by XRD and Raman spectroscopy. The XRD pattern of BiTeI flakes (Figure 2e) shows the same diffraction peak as that of the native bulk crystal, which matches the hexagonal $P3m1$ structure (PDF card: 98-007-9364).[6,49,54] This means that the LPE process preserves the crystallinity of the starting crystals without bringing about any additional phase. Figure 2f shows the Raman spectra of both BiTeI flakes and bulk crystals. The group theory predicts four active Raman modes, with the irreducible vibrational representation $\Gamma = 2A_1 + 2E$. (i.e., two E modes and two A_1 modes).[117,118] The peaks at 90 and 138 cm^{-1} are assigned to $A_1(1)$ and $A_1(2)$ modes, respectively, while E(1) and E(2) are found at 58 and 118 cm^{-1}. Contrary to previous studies on 2D BiTeI,[78,54] the presence of distinguishable Raman peaks in our exfoliated sample indicates a high crystallinity of the BiTeI flakes, in agreement with the XRD analysis. The crystalline nature of the BiTeI flakes is further confirmed by HRTEM measurements. Figure 2g reports a HRTEM image of two flakes overlapped, with the one on the right folded onto itself. The corresponding fast Fourier transform (FFT) of the HRTEM image (Figure 2h) confirms the single-crystalline nature of the flake and an exact [0001] orientation, which indicates that the bulk BiTeI is exfoliated perpendicular to the c axis of its hexagonal crystal structure, as expected by its layered structure.[6] Figure 2i shows a close-up view of the area outlined by a rectangle in Figure 2g, revealing an atomic arrangement as viewed from the [0001] direction.

Such an atomic arrangement matches the one expected for BiTeI in the same orientation (see the model at the top left corner of panel j). The HRTEM image of the fold on the edge of the flakes (Figure 2j) reveals that the flake is 14 or 15 BiTeI unit cells thick, with the individual monolayers spaced at ∼0.69 nm clearly resolved. Figure S3 shows the high-angle annular dark-field−scanning transmission electron microscopy

https://doi.org/10.1021/acsami.2c07704
ACS Appl. Mater. Interfaces 2022, 14, 34963−34974

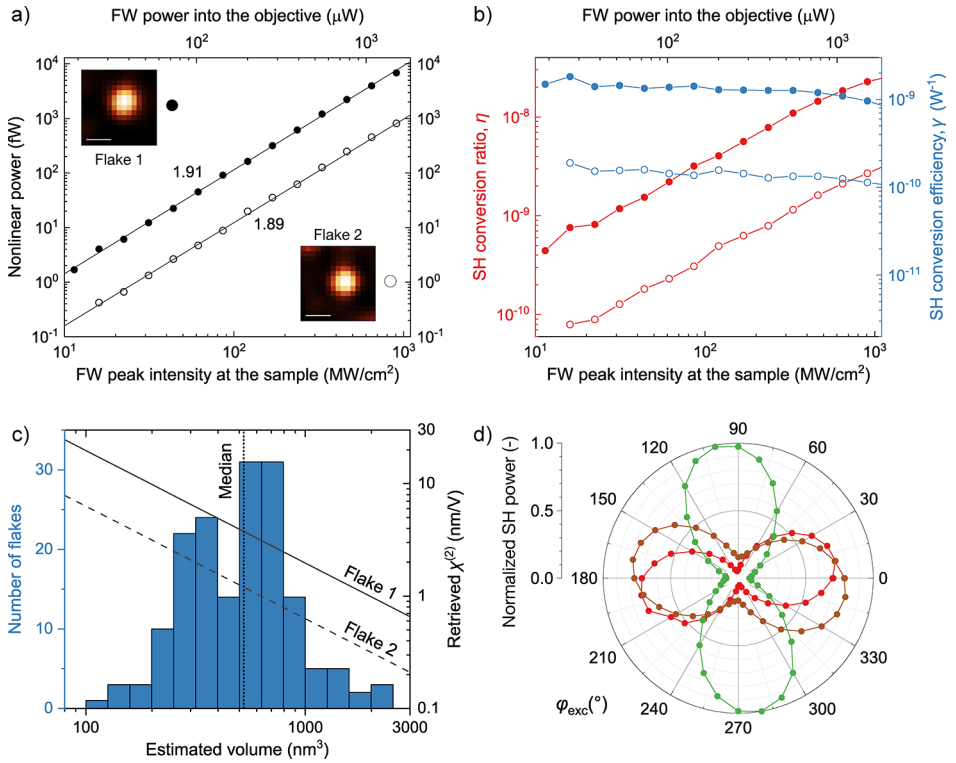

Figure 3. (a) SH power emitted by two few-layer BiTeI flakes (flake 1: solid dots and flake 2: empty dots) as a function of the FW peak intensity. Insets: confocal SH scans of the two flakes (the scale bar is 1 μm). The power law fits (solid lines, $P \propto I^p$) have an exponent p of 1.91 and 1.89, respectively. (b) Measured SH conversion ratio η (red) and conversion efficiency γ (blue) of the same two flakes as a function of the FW peak intensity. (c) (Histogram, left axis) retrieved number distribution of the flake volume; the median value of 524 nm^3 is indicated by the vertical dotted line. The overlaid lines (solid and dashed correspond to flakes with full and hollow symbols of panel a, respectively) show the analytical model of $|\chi^{(2)}(V)|$ expressed by eq 1. (d) Normalized SH power emitted by representative (individual) few-layer BiTeI flakes as a function of the pump polarization direction. Different colors indicate different flakes.

(HAADF−STEM) image of a BiTeI flake, together with the corresponding STEM−EDS maps of Bi, Te, and I. The quantitative elemental analysis results in a Bi:Te:I atomic ratio of 1:0.93:0.98 and a low atomic content of O (O:Bi atomic ratio of 0.17:1), which means that the LPE process in anhydrous IPA preserves the chemical integrity of the native crystal. It should also be noted that the use of IPA as a low-boiling point and high-vapor pressure solvent for the LPE process avoids solvent contamination of the flakes once deposited, as previously shown for other types of 2D materials (e.g., few-layer black phosphorous).[87]

To further confirm the non-centrosymmetric structure and crystalline quality of both bulk BiTeI and LPE-produced BiTeI crystals, their nonlinear optical properties are evaluated by SHG (Figures 3, S5, and S6). Figure 3 illustrates the SH emission by liquid phase-exfoliated BiTeI flakes drop-casted onto a SiO_2/Si substrate under pulsed excitation at the 1550 nm telecom wavelength (C band). Note, however, that we are not targeting any specific geometric (e.g., Mie-type) or material (e.g., excitonic) resonance. Indeed, the absence of sharp spectral features around the pump and SHG wavelength in the absorption spectrum (Figure 1d), together with the lack of the phase-matching requirement at subwavelength thicknesses, suggests that the nonlinear conversion efficiency reported below does not disperse strongly and therefore is amenable to broadband operation.

Figure 3a shows the nonlinear emission measured at 775 nm on two few-layer BiTeI flakes (named flake 1 and flake 2) and the power law fits. The quadratic dependence of the nonlinear power on the excitation power is the fingerprint of the second-order nonlinear optical process. The reported SH power represents the power emitted by the sample and entering the microscope objective, which has been quantified by considering the optical transmission or efficiency of all the elements in the detection path. The observed sample photodamage threshold is ∼1 GW cm^{-2} (Figure S5). The third-harmonic generation (THG) signal is detectable only above the photodamage threshold (Figure S5), so its fluence dependence is not reliable. Figure 3b shows the SH conversion ratio (η) and the conversion efficiency (γ) as a function of the fundamental wavelength (FW) peak intensity. The conversion ratio is defined as $\eta = P_{SH}/P_{FW}$, where P_{SH} and P_{FW} are the instantaneous (pulse peak) powers of SH emission and FW, respectively. Notably, η is expected to depend linearly on P_{FW}. The conversion efficiency is defined as $\gamma = P_{SH}/P_{FW}^2$ and characterizes the nonlinear emission of the material itself, being independent of the excitation (neither its power nor the repetition rate). Compared to the bulk nonlinear emission, BiTeI flakes show a 10-fold stronger nonlinear response (Figure S6). Recently, bulk BiTeI has been shown to possess a second-order nonlinear susceptibility $\chi^{(2)}$ as large as ∼400 pm V^{-1}. Therefore, by comparing the SH emission of our liquid-phase exfoliated BiTeI flakes with a native bulk, a $|\chi^{(2)}|$ of the order of 1 nm V^{-1} is reasonably expected. To estimate the $\chi^{(2)}$ of the material in its exfoliated form, we modeled the few-layer flake as an electric dipole lying flat on the planar SiO_2 surface. As described in Supporting Information, the analytical model accounts for the effect of the dielectric interface on the dipole

https://doi.org/10.1021/acsami.2c07704
ACS Appl. Mater. Interfaces 2022, 14, 34963−34974

radiation as well as for the finite solid angle of collection defined by the objective, leading to

$$\left|\chi^{(2)}(2\omega{:}\ \omega,\ \omega)\right| = \sqrt{\frac{3\pi\varepsilon_0 c_0^5 n_2}{f l_{\parallel}(2\omega)^4}}\ \frac{\sqrt{P_{\mathrm{det}}}}{I(\omega)V} \quad (1)$$

Here, ε_0 is the permittivity of vacuum, c_0 is the speed of light in vacuum, n_2 is the refractive index of air (equal to 1), $l_{\parallel}$ is a coefficient depending on the refractive index ratio of the interface and assumes that the dipole is parallel to the surface itself, V is the volume of the flake, and f is the fraction of emitted power collected by the objective (defined as $P_{\mathrm{det}} = fP_{\mathrm{tot}}$, where P_{tot} is the total SH power radiated by the dipole).

Now, the volume V of individual flakes is not known since AFM and TEM, as well as nonlinear optical measurements, are not correlated to single flakes. Nevertheless, to estimate the order of magnitude of $|\chi^{(2)}(V)|$, V can be retrieved by multiplying the TEM lateral size distribution (Figure 2c) with the median of the AFM thickness data (Figure 2d). Thus, Figure 3c reports $|\chi^{(2)}(V)|$ against the retrieved number distribution of V. According to eq 1, $\chi^{(2)}$ is inversely proportional to the V of the measured flake. By conservatively considering a large V of 1000 nm^3, one obtains $\chi^{(2)} = 2$ nm V^{-1} for flake 1 and 0.6 nm V^{-1} for flake 2. Such values are comparable to or larger than the typical susceptibilities of standard 3D semiconductors (e.g., 0.2 nm V^{-1} for GaAs) and similar to those previously reported for other 2D semiconductors in their monolayer form (e.g., 0.1−1 nm V^{-1} for TMDs).[95,97] Note that the buried interface with the Si wafer below the 285 nm thick SiO_2 substrate is not taken into account. Multiple reflections and interferences (i.e., Fabry−Pérot etaloning) contribute to the uncertainty affecting our estimate of $|\chi^{(2)}|$, which is, however, likely dominated by the uncertainty of V. Nevertheless, our results probe the potential of BiTeI, a representative layered Rashba-type material, as a nonlinear optical platform, both in its bulk and exfoliated form (i.e., single-/few-layer flakes).

As known from literature,[16] BiTeI crystals typically suffer from stacking faults. The surfaces in correspondence with such stacking faults may represent natural cleavage planes that are preferably subjected to the exfoliation process, leading to flakes with mixed surface terminations. It is therefore reasonable that the quality of the starting BiTeI crystal could affect the final morphological properties (e.g., thickness and lateral size) and structural characteristics of the LPE-produced BiTeI flakes. In this context, the dependence of the emitted nonlinear optical power on pump linear polarization can be used as a tool to probe such structural defects.[119,120] Although the nonlinear optical measurements are limited by diffraction to areas of ∼2 μm^2, Figure 3d reveals that the SH power reaches its maximum value for well-defined impinging pump polarizations. A marked dependence of the SH emission on the linear pump polarization indicates a lack of mirror symmetry in the 2D lattice structure material, which can be found in the crystal structure of monolayer BiTeI or few-layer BiTeI flakes with the absence of stacking faults. Therefore, these data support that the monocrystalline phase of few-layer flakes is being measured. Conversely, Figure S7 indicates that some other emitters show two preferential excitation directions for SHG. These emitters might be BiTeI flakes with a stacking fault, as intrinsically occurring in bulk BiTeI crystals,[10,16,121] as well as two distinct flakes within the laser spot. On the contrary, within the focused sample spot, the polarization response of multiple or aggregated flakes would be averaged to nearly isotropic due to their random orientations. Prospectively, the analysis of SHG dependence on the pump linear polarization may provide a valuable tool to evaluate the quality of both bulk and exfoliated BiTeI crystals, as well as other layered BiTeX.

CONCLUSIONS

In summary, we report the first ultrasonication-assisted LPE of BiTeI crystals, serving as a model for layered Rashba-type materials. By screening 12 different solvents, we elucidate the importance of minimizing the Gibbs free energy of the solvent/BiTeI crystal mixture to maximize the BiTeI exfoliation and dispersion. In more detail, this condition is achieved for solvents with surface tension γ^{sol} close to 28 mN m^{-1} (surface energy of 60 mJ m^{-2}) and the Hildebrand parameter (δ_{Hild}) between 19 and 25 MPa$^{0.5}$. By applying the Hansen solubility criterion, we estimate polar (δ_{P}), hydrogen bonding δ_{H}, and dispersion (δ_{D}) parameters for BiTeI in the range of 6−17, 6−19, and 15−18 MPa$^{0.5}$, respectively. Once the exfoliation of BiTeI crystals in the form of single-/few-layer flakes is optimized, we assess their morphological, structural, optical, and chemical characteristics through combined microscopic and spectroscopic techniques.

The non-centrosymmetric structure and crystallinity of both bulk and exfoliated BiTeI are further confirmed by their nonlinear optical response. Nonlinear frequency up-conversion of NIR light, demonstrated in this work, has high technological relevance as it enables detection with silicon-based devices. Together with the high-throughput solution-processed fabrication approach that we prove, our results suggest that exfoliated BiTeI can find application in functional inks and thin-film coatings for anti-counterfeiting schemes or night-vision devices. By modeling the BiTeI flakes as electric dipoles and determining their amplitude based on quantitative measurements, $|\chi^{(2)}|$ is estimated. Our results show that few-layer BiTeI can exhibit a large second-order nonlinear optical response ($\chi^{(2)} \sim 1$ nm V^{-1}), which is 10-fold more intense than that in bulk BiTeI crystals and possesses the same order of magnitude as that in other 2D materials in the monolayer form. Overall, our study provides guidelines for the LPE of Rashba-type polar BiTeX, highlighting its potential for advanced solution-processed applications, including spin-(orbi)tronic, thermoelectric, piezoelectric, and nonlinear optical systems, as well as other energy conversion devices.

ASSOCIATED CONTENT

Supporting Information

The Supporting Information is available free of charge at https://pubs.acs.org/doi/10.1021/acsami.2c07704.

Supplementary SEM−EDS characterizations; Hansen parameter analysis; supplementary HAADF−STEM characterizations; additional details of the SHG and THG experimental setup; and supplementary SHG and THG characterizations (PDF)

AUTHOR INFORMATION

Corresponding Authors

Sebastiano Bellani − *BeDimensional S.p.A., 16163 Genova, Italy*; Email: s.bellani@bedimensional.it

Francesco Bonaccorso − *Graphene Labs, Istituto Italiano di Tecnologia, 16163 Genova, Italy; BeDimensional S.p.A.,*

https://doi.org/10.1021/acsami.2c07704
ACS Appl. Mater. Interfaces 2022, 14, 34963−34974

16163 Genova, Italy; orcid.org/0000-0001-7238-9420; Email: f.bonaccorso@bedimensional.it

Authors

Gabriele Bianca − *Graphene Labs, Istituto Italiano di Tecnologia, 16163 Genova, Italy; Dipartimento di Chimica e Chimica Industriale, Università degli Studi di Genova, 16146 Genoa, Italy*

Chiara Trovatello − *Dipartimento di Fisica, Politecnico di Milano, 20133 Milano, Italy;* Present Address: Department of Mechanical Engineering, Columbia University, New York, New York 10027, United States

Attilio Zilli − *Dipartimento di Fisica, Politecnico di Milano, 20133 Milano, Italy;* orcid.org/0000-0003-1845-6850

Marilena Isabella Zappia − *BeDimensional S.p.A., 16163 Genova, Italy; Department of Physics, University of Calabria, Cosenza 87036, Italy*

Nicola Curreli − *Functional Nanosystems, Istituto Italiano di Tecnologia, 16163 Genova, Italy*

Irene Conticello − *BeDimensional S.p.A., 16163 Genova, Italy*

Joka Buha − *Nanochemistry Department, Istituto Italiano di Tecnologia, Genova 16163, Italy*

Marco Piccinni − *Graphene Labs, Istituto Italiano di Tecnologia, 16163 Genova, Italy; Dipartimento di Chimica e Chimica Industriale, Università degli Studi di Genova, 16146 Genoa, Italy*

Michele Ghini − *Functional Nanosystems, Istituto Italiano di Tecnologia, 16163 Genova, Italy*

Michele Celebrano − *Dipartimento di Fisica, Politecnico di Milano, 20133 Milano, Italy;* orcid.org/0000-0003-3336-3580

Marco Finazzi − *Dipartimento di Fisica, Politecnico di Milano, 20133 Milano, Italy;* orcid.org/0000-0002-9197-3654

Ilka Kriegel − *Functional Nanosystems, Istituto Italiano di Tecnologia, 16163 Genova, Italy;* orcid.org/0000-0002-0221-3769

Nikolas Antonatos − *Department of Inorganic Chemistry, University of Chemistry and Technology Prague, 16628 Prague 6, Czech Republic*

Zdeněk Sofer − *Department of Inorganic Chemistry, University of Chemistry and Technology Prague, 16628 Prague 6, Czech Republic;* orcid.org/0000-0002-1391-4448

Complete contact information is available at: https://pubs.acs.org/10.1021/acsami.2c07704

Author Contributions

G.B., C.T., M.I.Z., and S.B. conceived the idea of the work. N.A. and Z.S. synthesized and characterized the bulk BiTeI crystals. G.B., M.I.Z., S.B., N.C., I.C., J.B., M.P, M.G., and I.K. produced and characterized 2D BiTeI flakes. C.T., A.Z., M.F., and M.C. performed the nonlinear optical measurements and analyses. S.B., F.B., G.B., and C.T. wrote the article. F.B. and S.B. supervised the work. All authors have given approval to the final version of the article.

Funding

This project has received funding from the European Union's Horizon 2020 Research and Innovation programme under grant agreement no. 881603-GrapheneCore3. This project was supported by the Czech Science Foundation (GACR no. 20-16124J). N.C., M.G., and I.K. acknowledge the support of both European Union's Horizon 2020 European Research Council, under grant agreement no. 850875 (I.K.) (Light-DYNAMO), and European Union's Horizon 2020 Research and Innovation program under grant agreement no. 101017821 (I.K.) (LIGHT-CAP).

Notes

The authors declare no competing financial interest.

■ ACKNOWLEDGMENTS

The authors thank the Materials Characterization Facility—Istituto Italiano di Tecnologia—for the support in XRD data acquisition/analysis and Electron Microscopy facility—Istituto Italiano di Tecnologia—for the support in TEM data acquisition/analysis.

■ ABBREVIATIONS

2D, two-dimensional
3D, three-dimensional
AC, acetone
ACN, acetonitrile
AFM, atomic force microscopy
BF-TEM, bright-field transmission electron microscopy
CB, chlorobenzene
CF, chloroform
DMF, *N*,*N*-dimethylformamide
DRS, diffusive reflectance spectroscopy
EtOH, ethanol
EDS, energy-dispersive X-ray spectroscopy
EG, ethylene glycol
FFT, fast Fourier transform
FW, fundamental wavelength
HRTEM, high-resolution transmission electron microscopy
IPA, isopropanol
LPE, liquid-phase exfoliation
MeOH, methanol
NA, numerical aperture
NMP, *N*-methyl-2-pyrrolidone
SBS, sedimentation-based separation
SEM, scanning electron microscopy
SH, second harmonic
SHG, second-harmonic generation
TEM, transmission electron microscopy
THG, third-harmonic generation
TMDs, transition metal dichalcogenides
XRD, X-ray diffraction

■ REFERENCES

(1) Ishizaka, K.; Bahramy, M. S.; Murakawa, H.; Sakano, M.; Shimojima, T.; Sonobe, T.; Koizumi, K.; Shin, S.; Miyahara, H.; Kimura, A.; Miyamoto, K.; Okuda, T.; Namatame, H.; Taniguchi, M.; Arita, R.; Nagaosa, N.; Kobayashi, K.; Murakami, Y.; Kumai, R.; Kaneko, Y.; Onose, Y.; Tokura, Y. Giant Rashba-Type Spin Splitting in Bulk BiTeI. *Nat. Mater.* **2011**, *10*, 521−526.

(2) Bahramy, M. S.; Arita, R.; Nagaosa, N. Origin of Giant Bulk Rashba Splitting: Application to BiTeI. *Phys. Rev. B: Condens. Matter Mater. Phys.* **2011**, *84*, 041202.

(3) Landolt, G.; Eremeev, S. V.; Tereshchenko, O. E.; Muff, S.; Slomski, B.; Kokh, K. A.; Kobayashi, M.; Schmitt, T.; Strocov, V. N.; Osterwalder, J.; Chulkov, E. V.; Hugo Dil, J. Bulk and Surface Rashba Splitting in Single Termination BiTeCl. *New J. Phys.* **2013**, *15*, 085022.

(4) Chen, F.; Zhao, D.; Xiang, Z. J.; Shang, C.; Luo, X. G.; Pan, B. Y.; Li, S. Y.; Wu, T.; Chen, X. H. Quantum Oscillations in Rashba Semiconductor BiTeCl. *Phys. Rev. B: Condens. Matter Mater. Phys.* **2014**, *90*, 201202.

(5) Chen, Y. L.; Kanou, M.; Liu, Z. K.; Zhang, H. J.; Sobota, J. A.; Leuenberger, D.; Mo, S. K.; Zhou, B.; Yang, S.-L.; Kirchmann, P. S.; Lu, D. H.; Moore, R. G.; Hussain, Z.; Shen, Z. X.; Qi, X. L.; Sasagawa, T. Discovery of a Single Topological Dirac Fermion in the Strong Inversion Asymmetric Compound BiTeCl. *Nat. Phys.* **2013**, *9*, 704−708.
(6) Shevelkov, A. V.; Dikarev, E. V.; Shpanchenko, R. V.; Popovkin, B. A. Crystal Structures of Bismuth Tellurohalides BiTeX (X = Cl, Br, I) from X-Ray Powder Diffraction Data. *J. Solid State Chem.* **1995**, *114*, 379−384.
(7) Sakano, M.; Miyawaki, J.; Chainani, A.; Takata, Y.; Sonobe, T.; Shimojima, T.; Oura, M.; Shin, S.; Bahramy, M. S.; Arita, R.; Nagaosa, N.; Murakawa, H.; Kaneko, Y.; Tokura, Y.; Ishizaka, K. Three-Dimensional Bulk Band Dispersion in Polar BiTeI with Giant Rashba-Type Spin Splitting. *Phys. Rev. B: Condens. Matter Mater. Phys.* **2012**, *86*, 085204.
(8) Lee, J. S.; Schober, G. A. H.; Bahramy, M. S.; Murakawa, H.; Onose, Y.; Arita, R.; Nagaosa, N.; Tokura, Y. Optical Response of Relativistic Electrons in the Polar BiTeI Semiconductor. *Phys. Rev. Lett.* **2011**, *107*, 117401.
(9) Martin, C.; Mun, E. D.; Berger, H.; Zapf, V. S.; Tanner, D. B. Quantum Oscillations and Optical Conductivity in Rashba Spin-Splitting BiTeI. *Phys. Rev. B: Condens. Matter Mater. Phys.* **2013**, *87*, 041104.
(10) Crepaldi, A.; Moreschini, L.; Autès, G.; Tournier-Colletta, C.; Moser, S.; Virk, N.; Berger, H.; Bugnon, P.; Chang, Y. J.; Kern, K.; Bostwick, A.; Rotenberg, E.; Yazyev, O. V.; Grioni, M. Giant Ambipolar Rashba Effect in the Semiconductor BiTeI. *Phys. Rev. Lett.* **2012**, *109*, 096803.
(11) Eremeev, S. V.; Nechaev, I. A.; Koroteev, Y. M.; Echenique, P. M.; Chulkov, E. V. Ideal Two-Dimensional Electron Systems with a Giant Rashba-Type Spin Splitting in Real Materials: Surfaces of Bismuth Tellurohalides. *Phys. Rev. Lett.* **2012**, *108*, 246802.
(12) Eremeev, S. V.; Rusinov, I. P.; Nechaev, I. A.; Chulkov, E. V. Rashba Split Surface States in BiTeBr. *New J. Phys.* **2013**, *15*, 075015.
(13) Eremeev, S. V.; Nechaev, I. A.; Chulkov, E. V. Giant Rashba-Type Spin Splitting at Polar Surfaces of BiTeI. *JETP L.ett* **2012**, *96*, 437−444.
(14) Sakano, M.; Bahramy, M. S.; Katayama, A.; Shimojima, T.; Murakawa, H.; Kaneko, Y.; Malaeb, W.; Shin, S.; Ono, K.; Kumigashira, H.; Arita, R.; Nagaosa, N.; Hwang, H. Y.; Tokura, Y.; Ishizaka, K. Strongly Spin-Orbit Coupled Two-Dimensional Electron Gas Emerging near the Surface of Polar Semiconductors. *Phys. Rev. Lett.* **2013**, *110*, 107204.
(15) Crepaldi, A.; Cilento, F.; Zacchigna, M.; Zonno, M.; Johannsen, J. C.; Tournier-Colletta, C.; Moreschini, L.; Vobornik, I.; Bondino, F.; Magnano, E.; Berger, H.; Magrez, A.; Bugnon, P.; Autès, G.; Yazyev, O. V.; Grioni, M.; Parmigiani, F. Momentum and Photon Energy Dependence of the Circular Dichroic Photoemission in the Bulk Rashba Semiconductors BiTe X (X = I, Br, Cl). *Phys. Rev. B: Condens. Matter Mater. Phys.* **2014**, *89*, 125408.
(16) Fiedler, S.; El-Kareh, L.; Eremeev, S. V.; Tereshchenko, O. E.; Seibel, C.; Lutz, P.; Kokh, K. A.; Chulkov, E. V.; Kuznetsova, T. V.; Grebennikov, V. I.; Bentmann, H.; Bode, M.; Reinert, F. Defect and Structural Imperfection Effects on the Electronic Properties of BiTeI Surfaces. *New J. Phys.* **2014**, *16*, 075013.
(17) Butler, C. J.; Yang, H. H.; Hong, J. Y.; Hsu, S. H.; Sankar, R.; Lu, C. I.; Lu, H. Y.; Yang, K. H. O.; Shiu, H. W.; Chen, C. H.; Kaun, C. C.; Shu, G. J.; Chou, F. C.; Lin, M. T. Mapping Polarization Induced Surface Band Bending on the Rashba Semiconductor BiTeI. *Nat. Commun.* **2014**, *5*, 4066.
(18) Monserrat, B.; Vanderbilt, D. Temperature Dependence of the Bulk Rashba Splitting in the Bismuth Tellurohalides. *Phys. Rev. Mater.* **2017**, *1*, 054201.
(19) Rusinov, I. P.; Nechaev, I. A.; Eremeev, S. V.; Friedrich, C.; Blügel, S.; Chulkov, E. V. Many-Body Effects on the Rashba-Type Spin Splitting in Bulk Bismuth Tellurohalides. *Phys. Rev. B: Condens. Matter Mater. Phys.* **2013**, *87*, 205103.
(20) Bychkov, Y. A.; Rashba, E. I. Properties of a 2D Electron Gas with Lifted Spectral Degeneracy. *JETP L.ett* **1984**, *39*, 78.
(21) Zhu, Z.; Cheng, Y.; Schwingenschlögl, U. Orbital-Dependent Rashba Coupling in Bulk BiTeCl and BiTeI. *New J. Phys.* **2013**, *15*, 023010.
(22) Maaß, H.; Bentmann, H.; Seibel, C.; Tusche, C.; Eremeev, S. V.; Peixoto, T. R. F.; Tereshchenko, O. E.; Kokh, K. A.; Chulkov, E. V.; Kirschner, J.; Reinert, F. Spin-Texture Inversion in the Giant Rashba Semiconductor BiTeI. *Nat. Commun.* **2016**, *7*, 11621.
(23) Landolt, G.; Eremeev, S. V.; Koroteev, Y. M.; Slomski, B.; Muff, S.; Neupert, T.; Kobayashi, M.; Strocov, V. N.; Schmitt, T.; Aliev, Z. S.; Babanly, M. B.; Amiraslanov, I. R.; Chulkov, E. V.; Osterwalder, J.; Dil, J. H. Disentanglement of Surface and Bulk Rashba Spin Splittings in Noncentrosymmetric BiTeI. *Phys. Rev. Lett.* **2012**, *109*, 116403.
(24) Ye, L.; Checkelsky, J. G.; Kagawa, F.; Tokura, Y. Transport Signatures of Fermi Surface Topology Change in BiTeI. *Phys. Rev. B: Condens. Matter Mater. Phys.* **2015**, *91*, 201104.
(25) Ideue, T.; Ye, L.; Checkelsky, J. G.; Murakawa, H.; Kaneko, Y.; Tokura, Y. Thermoelectric Probe for Fermi Surface Topology in the Three-Dimensional Rashba Semiconductor BiTeI. *Phys. Rev. B: Condens. Matter Mater. Phys.* **2015**, *92*, 115144.
(26) Bell, C.; Bahramy, M. S.; Murakawa, H.; Checkelsky, J. G.; Arita, R.; Kaneko, Y.; Onose, Y.; Tokunaga, M.; Kohama, Y.; Nagaosa, N.; Tokura, Y.; Hwang, H. Y. Shubnikov−de Haas Oscillations in the Bulk Rashba Semiconductor BiTeI. *Phys. Rev. B: Condens. Matter Mater. Phys.* **2013**, *87*, 081109.
(27) Wang, C.-R.; Tung, J.-C.; Sankar, R.; Hsieh, C.-T.; Chien, Y.-Y.; Guo, G.-Y.; Chou, F. C.; Lee, W.-L. Magnetotransport in Copper-Doped Noncentrosymmetric BiTeI. *Phys. Rev. B: Condens. Matter Mater. Phys.* **2013**, *88*, 081104.
(28) Park, J.; Jin, K.-H.; Jo, Y. J.; Choi, E. S.; Kang, W.; Kampert, E.; Rhyee, J.-S.; Jhi, S.-H.; Kim, J. S. Quantum Oscillation Signatures of Pressure-Induced Topological Phase Transition in BiTeI. *Sci. Rep.* **2015**, *5*, 15973.
(29) Ideue, T.; Checkelsky, J. G.; Bahramy, M. S.; Murakawa, H.; Kaneko, Y.; Nagaosa, N.; Tokura, Y. Pressure Variation of Rashba Spin Splitting toward Topological Transition in the Polar Semiconductor BiTeI. *Phys. Rev. B: Condens. Matter Mater. Phys.* **2014**, *90*, 161107.
(30) Bordács, S.; Checkelsky, J. G.; Murakawa, H.; Hwang, H. Y.; Tokura, Y. Landau Level Spectroscopy of Dirac Electrons in a Polar Semiconductor with Giant Rashba Spin Splitting. *Phys. Rev. Lett.* **2013**, *111*, 166403.
(31) Ogawa, N.; Bahramy, M. S.; Murakawa, H.; Kaneko, Y.; Tokura, Y. Magnetophotocurrent in BiTeI with Rashba Spin-Split Bands. *Phys. Rev. B: Condens. Matter Mater. Phys.* **2013**, *88*, 035130.
(32) Bahramy, M. S.; Yang, B.-J.; Arita, R.; Nagaosa, N. Emergence of Non-Centrosymmetric Topological Insulating Phase in BiTeI under Pressure. *Nat. Commun.* **2012**, *3*, 679.
(33) Qi, Y.; Shi, W.; Naumov, P. G.; Kumar, N.; Sankar, R.; Schnelle, W.; Shekhar, C.; Chou, F.-C.; Felser, C.; Yan, B.; Medvedev, S. A. Topological Quantum Phase Transition and Superconductivity Induced by Pressure in the Bismuth Tellurohalide BiTeI. *Adv. Mater.* **2017**, *29*, 1605965.
(34) Jin, M. L.; Zhang, S. J.; Xing, L. Y.; Li, W. M.; Zhao, G. Q.; Wang, X. C.; Long, Y. W.; Li, X. D.; Bai, H. Y.; Gu, C. Z.; Jin, C. Q. Pressure-Induced Superconductivity and Quantum Phase Transitions in the Rashba Material BiTeCl. *J. Phys. Chem. Solids* **2019**, *128*, 211−217.
(35) Rusinov, I. P.; Menshchikova, T. V.; Sklyadneva, I. Y.; Heid, R.; Bohnen, K.-P.; Chulkov, E. V. Pressure Effects on Crystal and Electronic Structure of Bismuth Tellurohalides. *New J. Phys.* **2016**, *18*, 113003.
(36) Crassee, I.; Borondics, F.; Tran, M. K.; Autès, G.; Magrez, A.; Bugnon, P.; Berger, H.; Teyssier, J.; Yazyev, O. V.; Orlita, M.; Akrap, A. BiTeCl and BiTeBr: A Comparative High-Pressure Optical Study. *Phys. Rev. B* **2017**, *95*, 045201.
(37) Chen, Y.; Xi, X.; Yim, W.-L.; Peng, F.; Wang, Y.; Wang, H.; Ma, Y.; Liu, G.; Sun, C.; Ma, C.; Chen, Z.; Berger, H. High-Pressure Phase

https://doi.org/10.1021/acsami.2c07704
ACS Appl. Mater. Interfaces 2022, 14, 34963−34974

Transitions and Structures of Topological Insulator BiTeI. *J. Phys. Chem. C* **2013**, *117*, 25677−25683.
(38) Tan, L. Z.; Rappe, A. M. Enhancement of the Bulk Photovoltaic Effect in Topological Insulators. *Phys. Rev. Lett.* **2016**, *116*, 237402.
(39) Koo, H. C.; Kim, S. B.; Kim, H.; Park, T.-E.; Choi, J. W.; Kim, K.-W.; Go, G.; Oh, J. H.; Lee, D.-K.; Park, E.-S.; Hong, I.-S.; Lee, K.-J. Rashba Effect in Functional Spintronic Devices. *Adv. Mater.* **2020**, *32*, 2002117.
(40) Klimovskikh, I. I.; Shikin, A. M.; Otrokov, M. M.; Ernst, A.; Rusinov, I. P.; Tereshchenko, O. E.; Golyashov, V. A.; Sánchez-Barriga, J.; Varykhalov, A. Y.; Rader, O.; Kokh, K. A.; Chulkov, E. V. Giant Magnetic Band Gap in the Rashba-Split Surface State of Vanadium-Doped BiTeI: A Combined Photoemission and Ab Initio Study. *Sci. Rep.* **2017**, *7*, 3353.
(41) Kocsis, M.; Zheliuk, O.; Makk, P.; Tóvári, E.; Kun, P.; Tereshchenko, O. E.; Kokh, K. A.; Taniguchi, T.; Watanabe, K.; Ye, J.; Csonka, S. In Situ Tuning of Symmetry-Breaking Induced Non-Reciprocity in Giant-Rashba Semiconductor BiTeBr. *Phys. Rev. Res.* **2021**, *3*, 033253.
(42) Demkó, L.; Schober, G. A. H.; Kocsis, V.; Bahramy, M. S.; Murakawa, H.; Lee, J. S.; Kézsmárki, I.; Arita, R.; Nagaosa, N.; Tokura, Y. Enhanced Infrared Magneto-Optical Response of the Nonmagnetic Semiconductor BiTeI Driven by Bulk Rashba Splitting. *Phys. Rev. Lett.* **2012**, *109*, 167401.
(43) VanGennep, D.; Maiti, S.; Graf, D.; Tozer, S. W.; Martin, C.; Berger, H.; Maslov, D. L.; Hamlin, J. J. Pressure Tuning the Fermi Level through the Dirac Point of Giant Rashba Semiconductor BiTeI. *J. Phys. Condens. Matter* **2014**, *26*, 342202.
(44) Manchon, A.; Koo, H. C.; Nitta, J.; Frolov, S. M.; Duine, R. A. New Perspectives for Rashba Spin−Orbit Coupling. *Nat. Mater.* **2015**, *14*, 871−882.
(45) Tsutsui, K.; Murakami, S. Spin-Torque Efficiency Enhanced by Rashba Spin Splitting in Three Dimensions. *Phys. Rev. B: Condens. Matter Mater. Phys.* **2012**, *86*, 115201.
(46) Kovács-Krausz, Z.; Hoque, A. M.; Makk, P.; Szentpéteri, B.; Kocsis, M.; Fülöp, B.; Yakushev, M. V.; Kuznetsova, T. V.; Tereshchenko, O. E.; Kokh, K. A.; Lukács, I. E.; Taniguchi, T.; Watanabe, K.; Dash, S. P.; Csonka, S. Electrically Controlled Spin Injection from Giant Rashba Spin−Orbit Conductor BiTeBr. *Nano L.ett* **2020**, *20*, 4782−4791.
(47) Tournier-Colletta, C.; Autès, G.; Kierren, B.; Bugnon, P.; Berger, H.; Fagot-Revurat, Y.; Yazyev, O. V.; Grioni, M.; Malterre, D. Atomic and Electronic Structure of a Rashba p − n Junction at the BiTeI Surface. *Phys. Rev. B: Condens. Matter Mater. Phys.* **2014**, *89*, 085402.
(48) Li, X.; Sheng, Y.; Wu, L.; Hu, S.; Yang, J.; Singh, D. J.; Yang, J.; Zhang, W. Defect-Mediated Rashba Engineering for Optimizing Electrical Transport in Thermoelectric BiTeI. *npj Comput. Mater.* **2020**, *6*, 107.
(49) Wu, L.; Yang, J.; Zhang, T.; Wang, S.; Wei, P.; Zhang, W.; Chen, L.; Yang, J. Enhanced Thermoelectric Performance in the Rashba Semiconductor BiTeI through Band Gap Engineering. *J. Phys. Condens. Matter* **2016**, *28*, 085801.
(50) Xin, J.-Z.; Fu, C.-G.; Shi, W.-J.; Li, G.-W.; Auffermann, G.; Qi, Y.-P.; Zhu, T.-J.; Zhao, X.-B.; Felser, C. Synthesis and Thermoelectric Properties of Rashba Semiconductor BiTeBr with Intensive Texture. *Rare Met.* **2018**, *37*, 274−281.
(51) Wu, L.; Yang, J.; Wang, S.; Wei, P.; Yang, J.; Zhang, W.; Chen, L. Two-Dimensional Thermoelectrics with Rashba Spin-Split Bands in Bulk BiTeI. *Phys. Rev. B: Condens. Matter Mater. Phys.* **2014**, *90*, 195210.
(52) Kim, J.; Rabe, K. M.; Vanderbilt, D. Negative Piezoelectric Response of van Der Waals Layered Bismuth Tellurohalides. *Phys. Rev. B* **2019**, *100*, 104115.
(53) Wu, H.-J.; Yang, H.-R.; Rosales-Guzmán, C.; Gao, W.; Shi, B.-S.; Zhu, Z.-H. Vectorial Nonlinear Optics: Type-II Second-Harmonic Generation Driven by Spin-Orbit-Coupled Fields. *Phys. Rev. A* **2019**, *100*, 053840.
(54) Antonatos, N.; Kovalska, E.; Mazánek, V.; Veselý, M.; Sedmidubský, D.; Wu, B.; Sofer, Z. Electrochemical Exfoliation of Janus-like BiTeI Nanosheets for Electrocatalytic Nitrogen Reduction. *ACS Appl. Nano Mater.* **2021**, *4*, 590−599.
(55) Park, T.; Hong, J.; Shim, J. H. Enhancement of Giant Rashba Splitting in BiTeI under Asymmetric Interlayer Interaction. *J. Phys. Soc. Jpn.* **2020**, *89*, 044701.
(56) Novoselov, K. S.; Mishchenko, A.; Carvalho, A.; Castro Neto, A. H. 2D Materials and van Der Waals Heterostructures. *Science* **2016**, *353*, aac9439.
(57) Frisenda, R.; Navarro-Moratalla, E.; Gant, P.; Pérez De Lara, D.; Jarillo-Herrero, P.; Gorbachev, R. V.; Castellanos-Gomez, A. Recent Progress in the Assembly of Nanodevices and van Der Waals Heterostructures by Deterministic Placement of 2D Materials. *Chem. Soc. Rev.* **2018**, *47*, 53−68.
(58) Sunku, S. S.; Halbertal, D.; Engelke, R.; Yoo, H.; Finney, N. R.; Curreli, N.; Ni, G.; Tan, C.; McLeod, A. S.; Lo, C. F. B.; Dean, C. R.; Hone, J. C.; Kim, P.; Basov, D. N. Dual-Gated Graphene Devices for Near-Field Nano-Imaging. *Nano L.ett* **2021**, *21*, 1688−1693.
(59) Tajkov, Z.; Visontai, D.; Oroszlány, L.; Koltai, J. Uniaxial Strain Induced Topological Phase Transition in Bismuth−Tellurohalide−Graphene Heterostructures. *Nanoscale* **2019**, *11*, 12704−12711.
(60) Ma, Y.; Dai, Y.; Wei, W.; Li, X.; Huang, B. Emergence of Electric Polarity in BiTeX (X = Br and I) Monolayers and the Giant Rashba Spin Splitting. *Phys. Chem. Chem. Phys.* **2014**, *16*, 17603.
(61) Zhang, C.; Wang, S.; Zhang, H.; Feng, Y.; Tian, W.; Yan, Y.; Bian, J.; Wang, Y.; Jin, S.; Zakeeruddin, S. M.; Grätzel, M.; Shi, Y. Efficient Stable Graphene-Based Perovskite Solar Cells with High Flexibility in Device Assembling via Modular Architecture Design. *Energy Environ. Sci.* **2019**, *12*, 3585−3594.
(62) Das, T.; Balatsky, A. V. Engineering Three-Dimensional Topological Insulators in Rashba-Type Spin-Orbit Coupled Heterostructures. *Nat. Commun.* **2013**, *4*, 1972.
(63) Tajkov, Z.; Visontai, D.; Oroszlány, L.; Koltai, J. Topological Phase Diagram of BiTeX−Graphene Hybrid Structures. *Appl. Sci.* **2019**, *9*, 4330.
(64) Nechaev, I. A.; Eremeev, S. V.; Krasovskii, E. E.; Echenique, P. M.; Chulkov, E. V. Quantum Spin Hall Insulators in Centrosymmetric Thin Films Composed from Topologically Trivial BiTeI Trilayers. *Sci. Rep.* **2017**, *7*, 43666.
(65) Safeer, C. K.; Ingla-Aynés, J.; Herling, F.; Garcia, J. H.; Vila, M.; Ontoso, N.; Calvo, M. R.; Roche, S.; Hueso, L. E.; Casanova, F. Room-Temperature Spin Hall Effect in Graphene/MoS 2 van Der Waals Heterostructures. *Nano L.ett* **2019**, *19*, 1074−1082.
(66) Ghiasi, T. S.; Kaverzin, A. A.; Blah, P. J.; van Wees, B. J. Charge-to-Spin Conversion by the Rashba−Edelstein Effect in Two-Dimensional van Der Waals Heterostructures up to Room Temperature. *Nano L.ett* **2019**, *19*, 5959−5966.
(67) Benítez, L. A.; Savero Torres, W.; Sierra, J. F.; Timmermans, M.; Garcia, J. H.; Roche, S.; Costache, M. V.; Valenzuela, S. O. Tunable Room-Temperature Spin Galvanic and Spin Hall Effects in van Der Waals Heterostructures. *Nat. Mater.* **2020**, *19*, 170−175.
(68) Guo, S.-D.; Guo, X.-S.; Liu, Z.-Y.; Quan, Y.-N. Large Piezoelectric Coefficients Combined with High Electron Mobilities in Janus Monolayer XTeI (X = Sb and Bi): A First-Principles Study. *J. Appl. Phys.* **2020**, *127*, 064302.
(69) Stranks, S. D.; Plochocka, P. The Influence of the Rashba Effect. *Nat. Mater.* **2018**, *17*, 381−382.
(70) Waldrop, M. M. The chips are down for Moore's law. *Nature* **2016**, *530*, 144−147.
(71) Bonaccorso, F.; Sun, Z. Solution Processing of Graphene, Topological Insulators and Other 2d Crystals for Ultrafast Photonics. *Opt. Mater. Express* **2014**, *4*, 63.
(72) Bonaccorso, F.; Sun, Z.; Hasan, T.; Ferrari, A. C. Graphene Photonics and Optoelectronics. *Nat. Photonics* **2010**, *4*, 611−622.
(73) Björkman, T.; Gulans, A.; Krasheninnikov, A. V.; Nieminen, R. M. Van Der Waals Bonding in Layered Compounds from Advanced Density-Functional First-Principles Calculations. *Phys. Rev. Lett.* **2012**, *108*, 235502.

https://doi.org/10.1021/acsami.2c07704
ACS Appl. Mater. Interfaces 2022, 14, 34963−34974

(74) Bianca, G.; Zappia, M. I.; Bellani, S.; Sofer, Z.; Serri, M.; Najafi, L.; Oropesa-Nuñez, R.; Martín-García, B.; Hartman, T.; Leoncino, L.; Sedmidubský, D.; Pellegrini, V.; Chiarello, G.; Bonaccorso, F. Liquid-Phase Exfoliated GeSe Nanoflakes for Photoelectrochemical-Type Photodetectors and Photoelectrochemical Water Splitting. *ACS Appl. Mater. Interfaces* **2020**, *12*, 48598−48613.
(75) Zappia, M. I.; Bianca, G.; Bellani, S.; Serri, M.; Najafi, L.; Oropesa-Nuñez, R.; Martín-García, B.; Bouša, D.; Sedmidubský, D.; Pellegrini, V.; Sofer, Z.; Cupolillo, A.; Bonaccorso, F. Solution-Processed GaSe Nanoflake-Based Films for Photoelectrochemical Water Splitting and Photoelectrochemical-Type Photodetectors. *Adv. Funct. Mater.* **2020**, *30*, 1909572.
(76) Zacharia, R.; Ulbricht, H.; Hertel, T. Interlayer Cohesive Energy of Graphite from Thermal Desorption of Polyaromatic Hydrocarbons. *Phys. Rev. B: Condens. Matter Mater. Phys.* **2004**, *69*, 155406.
(77) Hajra, D.; Sailus, R.; Blei, M.; Yumigeta, K.; Shen, Y.; Tongay, S. Epitaxial Synthesis of Highly Oriented 2D Janus Rashba Semiconductor BiTeCl and BiTeBr Layers. *ACS Nano* **2020**, *14*, 15626−15632.
(78) Fülöp, B.; Tajkov, Z.; Pető, J.; Kun, P.; Koltai, J.; Oroszlány, L.; Tóvári, E.; Murakawa, H.; Tokura, Y.; Bordács, S.; Tapasztó, L.; Csonka, S. Exfoliation of Single Layer BiTeI Flakes. *2D Mater.* **2018**, *5*, 031013.
(79) Bonaccorso, F.; Bartolotta, A.; Coleman, J. N.; Backes, C. 2D-Crystal-Based Functional Inks. *Adv. Mater.* **2016**, *28*, 6136−6166.
(80) Hu, G.; Kang, J.; Ng, L. W. T.; Zhu, X.; Howe, R. C. T.; Jones, C. G.; Hersam, M. C.; Hasan, T. Functional Inks and Printing of Two-Dimensional Materials. *Chem. Soc. Rev.* **2018**, *47*, 3265−3300.
(81) Bellani, S.; Bartolotta, A.; Agresti, A.; Calogero, G.; Grancini, G.; Di Carlo, A.; Kymakis, E.; Bonaccorso, F. Solution-Processed Two-Dimensional Materials for next-Generation Photovoltaics. *Chem. Soc. Rev.* **2021**, *50*, 11870−11965.
(82) Jeong, G. H.; Sasikala, S. P.; Yun, T.; Lee, G. Y.; Lee, W. J.; Kim, S. O. Nanoscale Assembly of 2D Materials for Energy and Environmental Applications. *Adv. Mater.* **2020**, *32*, 1907006.
(83) Najafi, L.; Bellani, S.; Zappia, M. I.; Serri, M.; Oropesa-Nuñez, R.; Bagheri, A.; Beydaghi, H.; Brescia, R.; Pasquale, L.; Shinde, D. V.; Zuo, Y.; Drago, F.; Mosina, K.; Sofer, Z.; Manna, L.; Bonaccorso, F. Transition Metal Dichalcogenides as Catalysts for the Hydrogen Evolution Reaction: The Emblematic Case of "Inert" ZrSe 2 as Catalyst for Electrolyzers. *Nano Sel.* **2022**, *3*, 1069−1081.
(84) Padmajan Sasikala, S.; Lim, J.; Kim, I. H.; Jung, H. J.; Yun, T.; Han, T. H.; Kim, S. O. Graphene Oxide Liquid Crystals: A Frontier 2D Soft Material for Graphene-Based Functional Materials. *Chem. Soc. Rev.* **2018**, *47*, 6013−6045.
(85) Coleman, J. N.; Lotya, M.; O'Neill, A.; Bergin, S. D.; King, P. J.; Khan, U.; Young, K.; Gaucher, A.; De, S.; Smith, R. J.; Shvets, I. V.; Arora, S. K.; et al. Two-Dimensional Nanosheets Produced by Liquid Exfoliation of Layered Materials. *Science* **2011**, *331*, 568−571.
(86) Hansen, C. M. *Hansen Solubility Parameters A User's Handbook*; CRC press, 2013.
(87) Esau, A.; Rio, D.; Pellegrini, V.; Sun, H.; Buha, J.; Dinh, D. A.; Lago, E.; Ansaldo, A.; Capasso, A.; Manna, L.; Bonaccorso, F.; Del Rio Castillo, A. E.; Pellegrini, V.; Sun, H.; Buha, J.; Dinh, D. A.; Lago, E.; Ansaldo, A.; Capasso, A.; Manna, L.; Bonaccorso, F. Exfoliation of Few-Layer Black Phosphorus in Low-Boiling-Point Solvents and Its Application in Li-Ion Batteries. *Chem. Mater.* **2018**, *30*, 506−516.
(88) Garakani, M. A.; Bellani, S.; Pellegrini, V.; Oropesa-Nuñez, R.; Castillo, A. E.; Abouali, S.; Najafi, L.; Martín-García, B.; Ansaldo, A.; Bondavalli, P.; Demirci, C.; Romano, V.; Mantero, E.; Marasco, L.; Prato, M.; Bracciale, G.; Bonaccorso, F. Scalable Spray-Coated Graphene-Based Electrodes for High-Power Electrochemical Double-Layer Capacitors Operating over a Wide Range of Temperature. *Energy Storage Mater.* **2021**, *34*, 1−11.
(89) Hernandez, Y.; Nicolosi, V.; Lotya, M.; Blighe, F. M.; Sun, Z.; De, S.; McGovern, I. T.; Holland, B.; Byrne, M.; Gun'Ko, Y. K.; Boland, J. J.; Niraj, P.; Duesberg, G.; Krishnamurthy, S.; Goodhue, R.; Hutchison, J.; Scardaci, V.; Ferrari, A. C.; Coleman, J. N. High-Yield Production of Graphene by Liquid-Phase Exfoliation of Graphite. *Nat. Nanotechnol.* **2008**, *3*, 563−568.
(90) Kumar, M.; Gumber, S.; Lahon, S.; Jha, P. K.; Mohan, M. Third Harmonic Generation in Quantum Dot with Rashba Spin Orbit Interaction. *Eur. Phys. J. B* **2014**, *87*, 71.
(91) Lafalce, E.; Amerling, E.; Yu, Z. G.; Sercel, P. C.; Whittaker-Brooks, L.; Vardeny, Z. V. Rashba Splitting in Organic−Inorganic Lead−Halide Perovskites Revealed through Two-Photon Absorption Spectroscopy. *Nat. Commun.* **2022**, *13*, 483.
(92) Seyler, K. L.; Schaibley, J. R.; Gong, P.; Rivera, P.; Jones, A. M.; Wu, S.; Yan, J.; Mandrus, D. G.; Yao, W.; Xu, X. Electrical Control of Second-Harmonic Generation in a WSe2 Monolayer Transistor. *Nat. Nanotechnol.* **2015**, *10*, 407−411.
(93) Yin, X.; Ye, Z.; Chenet, D. A.; Ye, Y.; O'Brien, K.; Hone, J. C.; Zhang, X. Edge Nonlinear Optics on a MoS 2 Atomic Monolayer. *Science* **2014**, *344*, 488−490.
(94) Wang, H.; Qian, X. Giant Optical Second Harmonic Generation in Two-Dimensional Multiferroics. *Nano L.ett* **2017**, *17*, 5027−5034.
(95) Trovatello, C.; Marini, A.; Xu, X.; Lee, C.; Liu, F.; Curreli, N.; Manzoni, C.; Dal Conte, S.; Yao, K.; Ciattoni, A.; Hone, J.; Zhu, X.; Schuck, P. J.; Cerullo, G. Optical Parametric Amplification by Monolayer Transition Metal Dichalcogenides. *Nat. Photonics* **2021**, *15*, 6−10.
(96) Khan, A. R.; Zhang, L.; Ishfaq, K.; Ikram, A.; Yildrim, T.; Liu, B.; Rahman, S.; Lu, Y. Optical Harmonic Generation in 2D Materials. *Adv. Funct. Mater.* **2022**, *32*, 1−35.
(97) Wen, X.; Gong, Z.; Li, D. Nonlinear Optics of Two-Dimensional Transition Metal Dichalcogenides. *Infomatics* **2019**, *1*, 317−337.
(98) Zappia, M. I.; Bianca, G.; Bellani, S.; Curreli, N.; Sofer, Z.; Serri, M.; Najafi, L.; Piccinni, M.; Oropesa-Nuñez, R.; Marvan, P.; Pellegrini, V.; Kriegel, I.; Prato, M.; Cupolillo, A.; Bonaccorso, F. Two-Dimensional Gallium Sulfide Nanoflakes for UV-Selective Photoelectrochemical-Type Photodetectors. *J. Phys. Chem. C* **2021**, *125*, 11857−11866.
(99) Curreli, N.; Serri, M.; Zappia, M. I.; Spirito, D.; Bianca, G.; Buha, J.; Najafi, L.; Sofer, Z.; Krahne, R.; Pellegrini, V.; Bonaccorso, F. Liquid-Phase Exfoliated Gallium Selenide for Light-Driven Thin-Film Transistors. *Adv. Electron. Mater.* **2021**, *7*, 2001080.
(100) Del Rio Castillo, A. E.; Pellegrini, V.; Ansaldo, A.; Ricciardella, F.; Sun, H.; Marasco, L.; Buha, J.; Dang, Z.; Gagliani, L.; Lago, E.; Curreli, N.; Gentiluomo, S.; Palazon, F.; Prato, M.; Oropesa-Nuñez, R.; Toth, P. S.; Mantero, E.; Crugliano, M.; Gamucci, A.; Tomadin, A.; Polini, M.; Bonaccorso, F. High-Yield Production of 2D Crystals by Wet-Jet Milling. *Mater. Horiz.* **2018**, *5*, 890−904.
(101) Bellani, S.; Petroni, E.; Del Rio Castillo, A. E.; Curreli, N.; Martín-García, B.; Oropesa-Nuñez, R.; Prato, M.; Bonaccorso, F. Scalable Production of Graphene Inks via Wet-Jet Milling Exfoliation for Screen-Printed Micro-Supercapacitors. *Adv. Funct. Mater.* **2019**, *29*, 1807659.
(102) Beydaghi, H.; Bellani, S.; Najafi, L.; Oropesa-Nuñez, R.; Bianca, G.; Bagheri, A.; Conticello, I.; Martín-García, B.; Kashefi, S.; Serri, M.; Liao, L.; Sofer, Z.; Pellegrini, V.; Bonaccorso, F. Sulfonated NbS 2 -Based Proton-Exchange Membranes for Vanadium Redox Flow Batteries. *Nanoscale* **2022**, *14*, 6152−6161.
(103) Backes, C.; Abdelkader, A. M.; Alonso, C.; Andrieux-Ledier, A.; Arenal, R.; Azpeitia, J.; Balakrishnan, N.; Banszerus, L.; et al. Production and Processing of Graphene and Related Materials. *2D Mater.* **2020**, *7*, 22001.
(104) Curreli, N.; Serri, M.; Spirito, D.; Lago, E.; Petroni, E.; Martín-García, B.; Politano, A.; Gürbulak, B.; Duman, S.; Krahne, R.; Pellegrini, V.; Bonaccorso, F. Liquid Phase Exfoliated Indium Selenide Based Highly Sensitive Photodetectors. *Adv. Funct. Mater.* **2020**, *30*, 1908427.
(105) Maragó, O. M.; Bonaccorso, F.; Saija, R.; Privitera, G.; Gucciardi, P. G.; Iatì, M. A.; Calogero, G.; Jones, P. H.; Borghese, F.; Denti, P.; Nicolosi, V.; Ferrari, A. C. Brownian Motion of Graphene. *ACS Nano* **2010**, *4*, 7515.

https://doi.org/10.1021/acsami.2c07704
ACS Appl. Mater. Interfaces 2022, 14, 34963−34974

(106) Najafi, L.; Oropesa-Nuñez, R.; Bellani, S.; Martín-García, B.; Pasquale, L.; Serri, M.; Drago, F.; Luxa, J.; Sofer, Z.; Sedmidubský, D.; Brescia, R.; Lauciello, S.; Zappia, M. I.; Shinde, D. V.; Manna, L.; Bonaccorso, F. Topochemical Transformation of Two-Dimensional VSe 2 into Metallic Nonlayered VO 2 for Water Splitting Reactions in Acidic and Alkaline Media. *ACS Nano* **2022**, *16*, 351−367.
(107) Yang, L.; Miklavcic, S. J. Revised Kubelka−Munk Theory III A General Theory of Light Propagation in Scattering and Absorptive Media. *J. Opt. Soc. Am. A* **2005**, *22*, 1866.
(108) Najafi, L.; Taheri, B.; Martín-García, B.; Bellani, S.; Di Girolamo, D.; Agresti, A.; Oropesa-Nunìez, R.; Pescetelli, S.; Vesce, L.; Calabrò, E.; Prato, M.; Del Rio Castillo, A. E.; Di Carlo, A.; Bonaccorso, F. MoS2 Quantum Dot/Graphene Hybrids for Advanced Interface Engineering of a CH3NH3PbI3 Perovskite Solar Cell with an Efficiency of over 20. *ACS Nano* **2018**, *12*, 10736−10754.
(109) Bonaccorso, F.; Lombardo, A.; Hasan, T.; Sun, Z.; Colombo, L.; Ferrari, A. C. Production and Processing of Graphene and 2d Crystals. *Mater. Today* **2012**, *15*, 564−589.
(110) Najafi, L.; Bellani, S.; Oropesa-Nuñez, R.; Ansaldo, A.; Prato, M.; Del Rio Castillo, A. E.; Bonaccorso, F. Doped-MoSe2 Nanoflakes/3d Metal Oxide−Hydr(Oxy)Oxides Hybrid Catalysts for PH-Universal Electrochemical Hydrogen Evolution Reaction. *Adv. Energy Mater.* **2018**, *8*, 1801764.
(111) Venkatram, S.; Kim, C.; Chandrasekaran, A.; Ramprasad, R. Critical Assessment of the Hildebrand and Hansen Solubility Parameters for Polymers. *J. Chem. Inf. Model.* **2019**, *59*, 4188−4194.
(112) Barton, A. F. M. Solubility Parameters. *Chem. Rev.* **1975**, *75*, 731−753.
(113) Makhnev, A. A.; Nomerovannaya, L. V.; Kuznetsova, T. V.; Tereshchenko, O. E.; Kokh, K. A. Optical Properties of BiTeI Semiconductor with a Strong Rashba Spin-Orbit Interaction. *Opt. Spectrosc.* **2014**, *117*, 764−768.
(114) Boutinaud, P. Revisiting the Spectroscopy of the Bi 3+ Ion in Oxide Compounds. *Inorg. Chem.* **2013**, *52*, 6028−6038.
(115) Blasse, G.; Bril, A. Investigations on Bi^{3+} -Activated Phosphors. *J. Chem. Phys.* **1968**, *48*, 217−222.
(116) Blasse, G. The Ultraviolet Absorption Bands of Bi^{3+} and Eu^{3+} in Oxides. *J. Solid State Chem.* **1972**, *4*, 52−54.
(117) Sklyadneva, I. Y.; Heid, R.; Bohnen, K.-P.; Chis, V.; Volodin, V. A.; Kokh, K. A.; Tereshchenko, O. E.; Echenique, P. M.; Chulkov, E. V. Lattice Dynamics of Bismuth Tellurohalides. *Phys. Rev. B: Condens. Matter Mater. Phys.* **2012**, *86*, 094302.
(118) Tran, M. K.; Levallois, J.; Lerch, P.; Teyssier, J.; Kuzmenko, A. B.; Autès, G.; Yazyev, O. V.; Ubaldini, A.; Giannini, E.; van der Marel, D.; Akrap, A. Infrared- and Raman-Spectroscopy Measurements of a Transition in the Crystal Structure and a Closing of the Energy Gap of BiTeI under Pressure. *Phys. Rev. Lett.* **2014**, *112*, 047402.
(119) Hristu, R.; Stanciu, S. G.; Tranca, D. E.; Polychroniadis, E. K.; Stanciu, G. A. Identification of Stacking Faults in Silicon Carbide by Polarization-Resolved Second Harmonic Generation Microscopy. *Sci. Rep.* **2017**, *7*, 4870.
(120) Cunha, R.; Cadore, A.; Ramos, S. L. L. M.; Watanabe, K.; Taniguchi, T.; Kim, S.; Solntsev, A. S.; Aharonovich, I.; Malard, L. M. Second Harmonic Generation in Defective Hexagonal Boron Nitride. *J. Phys. Condens. Matter* **2020**, *32*, 19LT01.
(121) Kohsaka, Y.; Kanou, M.; Takagi, H.; Hanaguri, T.; Sasagawa, T. Imaging Ambipolar Two-Dimensional Carriers Induced by the Spontaneous Electric Polarization of a Polar Semiconductor BiTeI. *Phys. Rev. B: Condens. Matter Mater. Phys.* **2015**, *91*, 245312.

https://doi.org/10.1021/acsami.2c07704
ACS Appl. Mater. Interfaces 2022, 14, 34963−34974